Magnetic Resonance Imaging 62 (2019) 174–180

Contents lists available at ScienceDirect

Magnetic Resonance Imaging

journal homepage: www.elsevier.com/locate/mri

Case report

Effect of spiral undersampling patterns on FISP MRF parameter maps

Gregor Körzdörfer[a,b,*], Josef Pfeuffer[a], Thomas Kluge[a], Matthias Gebhardt[a], Bernhard Hensel[b], Craig H. Meyer[c], Mathias Nittka[a]

[a] Siemens Healthcare, Erlangen, Germany
[b] Friedrich-Alexander-Universität Erlangen-Nürnberg, Erlangen, Germany
[c] Departments of Biomedical Engineering and Radiology, University of Virginia, Charlottesville, VA, USA

ARTICLE INFO

Keywords:
Quantitative MRI
Magnetic Resonance Fingerprinting
Spiral imaging

ABSTRACT

Purpose: Artifacts arising from undersampling are not always treatable as incoherent noise for the pattern matching process in Magnetic Resonance Fingerprinting (MRF). To estimate the effect of undersampling artifacts on MRF quantitative results, spiral sampling trajectories and their temporal variation is examined.
Methods: The effect of sampling trajectories and their variation during the MRF experiment was assessed by characterizing aliasing artifacts. Temporal rearrangements of sampling trajectories were tested and evaluated in simulations and scans of phantoms and in a volunteer brain.
Results: Results show that some temporal variations of sampling patterns can lead to spatial biases in MRF parameter maps. Observed effects are consistent with derived performance indicators for different interleaving schemes, leading to substantially improved MRF sampling patterns.
Conclusion: With the help of the presented simulation framework, MRF implementations can be investigated and improved. This was demonstrated for a spiral FISP (Fast imaging with steady-state free precession) MRF implementation, where a significantly improved interleaving scheme was identified, and confirmed by experiment.

1. Introduction

Routine clinical MRI involves creating anatomical images of different tissue contrast. Pathologies and tissue changes can be assessed because they show up with a different brightness in the image. Most common image contrasts are determined by the longitudinal (T1) and the transverse (T2) relaxation times of tissues. For multiple reasons it would be attractive to directly measure the relaxation times, i.e. to replace the relative image brightness by a quantitative and reproducible parameter. Several techniques have been developed to measure relaxation times but long scan times and high sensitivity to confounding factors have prevented them from widespread clinical use [1].

Magnetic Resonance Fingerprinting (MRF) tries to overcome these drawbacks by employing a technique that directly measures both relaxation parameters in a single experiment in an efficient way. Instead of sampling exponential signal decay, a pseudo-random excitation pattern generates a non-steady-state signal. These signals can be assigned to relaxation times by comparing them with a physical signal model. MRF is mainly implemented by using gradient echo sequences, such as TrueFISP (True Fast imaging with steady-state free precession, 2), FISP (Fast imaging with steady-state free precession, 3) or combinations of FISP and FLASH (fast low angle shot, 4). The comparison with the physical model is done by comparing the acquired signals with a pre-computed set of simulated signals which is called a dictionary [2–4].

MRF acquisitions can be substantially shortened by means of spatial undersampling. Established techniques for undersampling in MRF are single-shot spirals [2,3] and radial [4] scanning. In principle, every undersampling strategy including conventional Cartesian sampling using GRAPPA (GeneRalized Autocalibrating Partial Parallel Acquisition), SENSE (Sensitivity Encoding), partial-Fourier or elliptical scanning can be utilized. The undersampling factors can be considerably higher than the ones applied in conventional MRI. The basic assumption underlying fast MRF is the hypothesis that a spatial undersampling scheme leads to incoherent aliasing artifacts in the time domain. Accordingly, the pattern matching process is assumed to be unaffected by these artifacts [2]. Originally, a simple ascending reordering was used for MRF. Here, a limited number of spirals n is generated by rotating an initially designed spiral. For every data acquisition, the spiral is rotated

Abbreviations: MRF, Magnetic Resonance Fingerprinting; FISP, Fast imaging with steady-state free precession; TrueFISP, True Fast imaging with steady-state free precession; FLASH, fast low angle shot; GRAPPA, GeneRalized Autocalibrating Partial Parallel Acquisition; SENSE, Sensitivity Encoding

* Corresponding author at: Siemens Healthcare GmbH, Allee am Roethelheimpark 2, 91052 Erlangen, Germany.
E-mail address: koerzdoerfer@siemens-healthineers.com (G. Körzdörfer).

https://doi.org/10.1016/j.mri.2019.01.011
Received 17 October 2018; Received in revised form 11 January 2019; Accepted 12 January 2019

by an angle $\alpha = \frac{360^{\circ}}{n}$ [2,3,5,6]. Other MRF implementations use a golden-angle increment for rotation of the spirals [7,8]. To improve the parameter map quality, the MRF data can also be reconstructed using iterative or low-rank methods [9–12].

The presented work aims to study the effect of interleave order on aliasing artifacts and resulting quantitative maps in a prototype FISP MRF implementation applying single-shot spiral sampling. Experiments were performed on phantoms and compared to results from numerical simulations. With insights gained and further theory derived from these experiments, in-vivo spiral FISP MRF measurements in the human brain could be significantly improved, compared to the originally proposed ascending order of spirals. Preliminary results from this work have been published in abstract form [13,14], and some of the methods have been submitted as a patent application [15].

2. Materials and methods

For all simulations and experiments in this work, a prototype FISP MRF implementation, based on the signal encoding scheme from Jiang et al. [3], was used. This implementation is briefly described in the following section.

After the application of an adiabatic inversion pulse, a train of slice selective RF pulses with varying flip angles and repetition times (TR) is applied. In contrast to conventional MRI, MRF encoding schemes are designed to yield non-steady-state signals exhibiting well differentiable temporal characteristics with respect to spins with different relaxation rates. Each TR encodes one image with a short spiral read-out of approx. 6 ms, resulting in a series of strongly undersampled images.

For the experimental and theoretical investigations in this work, a train of 3000 RF pulses was used. A base TR of 12 ms was chosen with an additional TR increment changing from echo to echo as in [3]. Two different spiral trajectories were used to sample the two-dimensional k-space, one with a dual-density design [16] and the other one with constant density. The dual-density spiral was designed for a field of view of 300 mm, a matrix size of 256 and an undersampling factor of 24 in the center of k-space with a transition to 48 in the peripheral regions of k-space. A constant-density spiral was designed for a FOV of 400 mm and a matrix size of 352 with a constant undersampling factor of 48. Spiral trajectories were corrected using the generalized eddy-current model by Tan and Meyer [17].

In order to produce undersampling artifacts varying in the time domain, 48 spiral interleaves were generated that are rotated versions of the original spiral interleaf. Each of the 48 spiral interleaves is rotated by an angle $\varphi = \mathrm{i} * 360/48^{\circ}$ against the original spiral interleaf ($i = 0$), where $\mathrm{i} \in \{0;1;\ldots;47\}$ denotes the index of the spiral interleaf.

To constrain the problem, focus was placed on recurrent interleaf reordering (ILR) patterns with the length of 48. The straight forward approach is to use a simple ILR such as [0;1;2;…;47] which is called ascending mode, or similarly the descending mode [47;46;45;…;0]. Furthermore, it is possible to define interleaf reorderings, which apply an index increment of consecutive spirals. These are called STEP-x ILRs, with x denoting the index increment of consecutive spirals. For example, STEP–1 is identical to ascending mode, STEP–2 is [0;2;4;6;…], and STEP–24 is [0;24;1;25;…]. The index is incremented by 1 when a previously used interleaf index is reached, in order to use all indices. As an additional parameter, the starting index (ILR offset) of the first spiral interleaf that is played out was varied.

'Sinc' shaped RF pulses with a time-bandwidth product of 8, duration of 2000 μs and a slice thickness of 5 mm are used for excitation except for the adiabatic inversion pulse. To mitigate the influence arising from inhomogeneities of the transmit RF field B_1+ [18,19], a B_1+ correction was applied. Here a B_1+ prescan [20] is acquired, and the relative B_1+ value determines a subdictionary for the matching process, calculated with the corresponding relative B_1+. This method is similar to previously reported prescan-based B_1+ corrections for MRF [21,22].

The impact of the different sampling trajectory implementations on MRF parameter maps can be investigated by performing simulations using the spatial response function (SRF) [23]. While the point spread function describes how signal from one pixel is distributed to other pixels, the SRF describes how signal in one pixel is collected from other pixels. Each pixel's signal was computed by multiplying the signal map and the pixel's SRF. A two-dimensional digital phantom incorporating a B_1+ map and coil sensitivities derived from a scan of a real phantom was used, neglecting other possible influences on the signal. The real phantom was an oil-filled sphere to minimize dielectric effects on the transmit field. Relaxation times of the oil were determined by spatially averaging results over the homogenous phantom from an MRF scan. MRF scans were acquired with both spiral trajectories and different spiral interleaf reorderings and compared to the corresponding simulated MRF parameter maps. All data were acquired on a 3 T whole-body scanner (MAGNETOM Skyra, Siemens Healthcare, Germany).

STEP-x spiral ILRs were also tested on a human head-shaped phantom filled with agarose. The signals resulting from the experiments were compared to the non-undersampled signal, which was approximated as the fingerprint with the mean T1 and T2 relaxation times over the phantom. A subtraction of the measured signal from the best-matching dictionary entry yields the residuals for every pixel caused by aliasing. Since the spiral reordering is repeated every 48 echoes, the residuals can be divided into segments, each 48 time points long and plotted one above the other. This procedure was done for several ILRs, and the mean value over the segmented residuals of each ILR was calculated. A Fourier transform of the mean of the segmented residuals reveals their frequency composition. Rearranging the mean of the segmented residuals by index of the spiral interleaf leads to spiral-interleaf-specific aliasing noise rather than temporal aliasing noise.

Furthermore, the mean residual per spiral interleaf for each pixel can be rearranged in a specific order similar to the STEP-x patterns, which leads to an artificial residual pattern. This approach provides an easier means for analyzing the characteristics of residuals without the need for measuring with different spiral ILRs. Frequency analyses of these artificial residual patterns were carried out for all STEP-x ILRs, and a score for estimating the effects on pattern matching was introduced. The sum of squares over the pairwise differences of the spectra of fingerprints was taken on the exhaustive dictionary. The result characterizes the fingerprints' frequencies contribution to the encoding of tissue parameters. This spectrum was used as a weighting function for the spectra of the residuals. The residuals' frequencies are thus weighted according to their contribution to the encoding of tissue parameters. The hypothesis underlying this score is that residuals consisting of different frequencies than the ones contributing to the encoding of tissue parameters have a vanishing correlation with all dictionary atoms, whereas other frequency residuals potentially distort the signal in a way that the pattern matching results are biased.

A further experimental criterion for evaluating the effects of a reordering mode upon spatial biases is to compare two parameter maps from acquisitions with the same reordering mode. The two acquisitions differ only in the starting point of their reordering. One starts at index n and the other one at n + 24, yielding maximum phase difference of residuals. Resulting difference maps should be zero if the reordering scheme is well suited i.e. the result does not vary in spatial position.

ILR schemes were tested and evaluated regarding the criteria described above. The pattern performing best was also tested in vivo on a volunteer brain and compared to the conventional STEP-1 ILR schemes. The data from in vivo acquisitions were also reconstructed using AIR-MRF [11], a method for iterative reconstruction of MRF data that employs fingerprint compression, additional spatial regularization and FLANN [24,25], an accelerated dictionary search methods. One tree was used for FLANN and leaves to check was set to 512 and ten iterations were used for AIR-MRF.

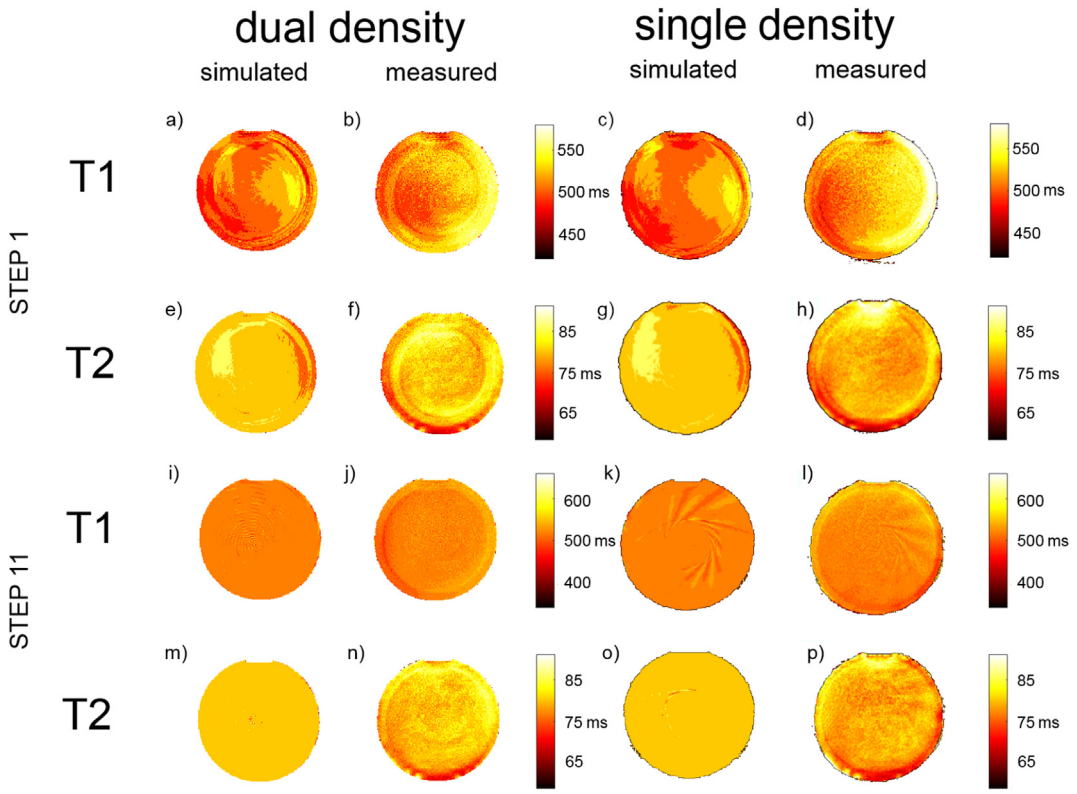

Fig. 1. Parameter maps of an oil-filled sphere calculated from simulated and measured MRF acquisitions. Left side shows results for the dual-density spiral, right side for the constant-density spiral. a) b) c) d) are T1 maps from ascending (STEP-1) reordering mode and e) f) g) h) the respective T2 maps. i) j) k) l) are T1 maps from STEP-11 reordering mode and m) n) o) p) the respective T2 maps.

3. Results

Fig. 1 displays resulting parameter maps from simulated spiral MRF on the oil-filled sphere. For comparison, the parameter maps from real MRF experiments on the phantom are also depicted in this figure. With ILR STEP-1, shading can be observed in parameter maps, especially the T1 maps, with both spiral variants. When using the ILR STEP-11, this effect is largely mitigated. The T1 maps acquired using a single-density spiral and ILR STEP-11 show a remarkable spiral-like pattern, which can be reproduced with the simulations. Shading is also visible in the T2 maps, but since T2 map errors are also influenced strongly by B1 inhomogeneities [6,18,19] and noise, they are harder to reproduce by simulation. Nevertheless, the artificial T2 maps from simulations show a similar pattern to those from MRF experiments.

Results from subtracting true and measured signal are exhibited in Fig. 2. Fig. 2a) illustrates how this is carried out in detail. One pixel in the phantom was analyzed using acquisitions with different interleaf reordering schemes (Fig. 2b)–e)). The residuals were reordered by index of the spiral interleaf instead of a temporal order, and the mean residual for each spiral interleaf was calculated (Fig. 2f)). These spiral-interleaf-specific mean residuals from MRF acquisitions with different ILR schemes deviate very little from each other.

Calculating a pixel-specific mean residual curve was repeated for all pixels in the phantom. Since this mean is independent of the reordering scheme and mainly depends on the spiral interleaf, the mean residual curve of each pixel can be rearranged by ILR patterns. A Fourier analysis of the artificially reordered residuals reveals the 'residual spectra'. Weighting the resulting spectrum by a function which frequencies contribute to the encoding (Fig. 3b)) gives a metric that is called weighted frequency score. Frequencies are weighted according to their contribution to the encoding of tissue parameters. The resulting mean score of all pixels within the phantom for STEP-x interleaf reorderings is depicted in Fig. 3c).

The findings can be transferred to MRF measurements of the human brain. Parameter and difference maps are depicted in Fig. 4. STEP-11 parameter maps with offset 0 and 24 and the corresponding difference maps exhibit almost no spatial biases, whereas both STEP-1 difference maps show a strong bias that is rotated with ILR offsets. With AIR-MRF the artifacts when using STEP-1 are significantly reduced compared to the conventional reconstruction. STEP-11 acquisitions with AIR-MRF exhibit the smallest difference between offset 0 and 24. T1 values of all parameter maps in four ROIs in the brain, and corresponding T2 values are displayed in Table 1.

4. Discussion

Parameter maps of the oil-filled sphere resulting from simulations show similar spatial biases as the actual measured maps. This result demonstrates that the biases in MRF parameter maps are mainly influenced by the reordering of aliasing artifacts rather than other potential factors, such as signal deviations by eddy currents, which were not incorporated in the simulation. FISP MRF implementations are not as sensitive to deviations of expected gradient moments as TrueFISP [2,26] implementations, since FISP does not require fully balanced gradients at the end of each TR.

The residuals of different reorderings in the phantom experiment are repetitive: when reordering the mean of the segments per ILR by spiral interleaf index, almost the same curves are generated for the four ILR patterns tested on the phantom. Within the scope of our experiments, the spiral-interleaf-specific residuals dominate all other sources of signal errors and are almost uninfluenced by ILR patterns.

Comparing these results to the weighted frequency score (Fig. 3) of the STEP-x reorderings reveals that the occurrence of spatial biases in parameter maps in the homogenous phantom corresponds to the frequency spectrum of the aliasing artifacts. For this phantom, the best STEP-x reordering was found to be STEP-11. This reordering also

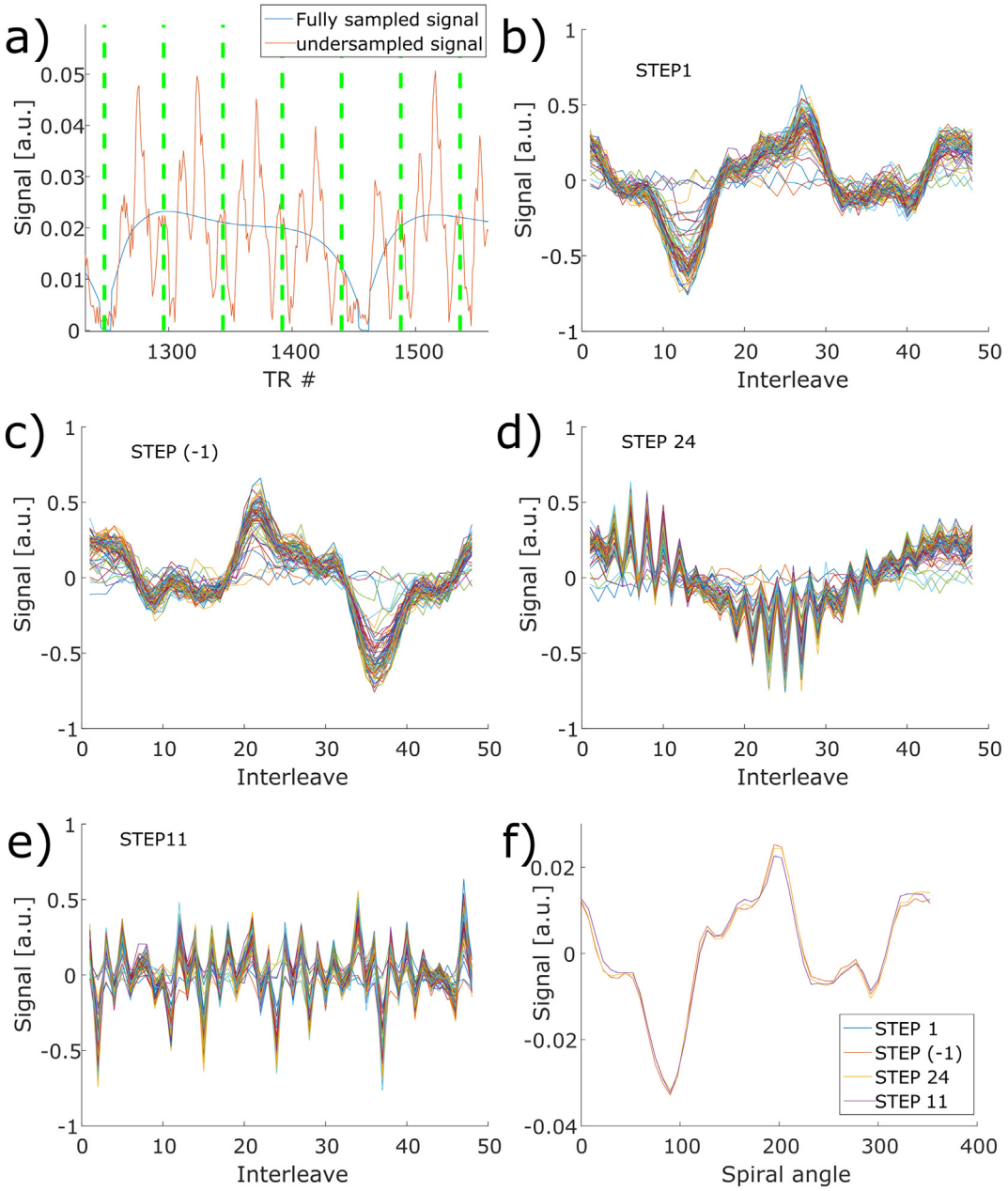

Fig. 2. a) True (fully sampled) and measured undersampled signal from one pixel (excerpt of the whole temporal signal course). Dashed green vertical lines are shown every 48 echoes. The subtraction of measured and true signal, which is the residual is divided in these sections. In each of these sections the Reordering is the same. b) to e): Residuals from subtracting true and measured signals for several reorderings. Since the reorderings are recurrent, residuals are plotted one above the other. For simplicity, only the real part of the residuals is shown here; a similar behavior can be observed for the imaginary part. b) ascending (STEP-1) reordering, c) descending (STEP-(-1)) reordering, d) alternating (STEP-24) and e) STEP-11 reordering. f) shows the mean real value of the 48-time-point-long residuals for each reordering. The residuals are plotted against the spiral interleaf angle. (For interpretation of the references to color in this figure legend, the reader is referred to the web version of this article.)

produces the residuals with the fewest frequencies contributing to the encoding of tissue parameters. This finding can be explained by considering the design of the fingerprints. The signal in FISP MRF is designed to vary slowly and subsequently to have a low frequency. High-frequency residuals as produced by the STEP-11 scheme exhibit a lower correlation with the dictionary atoms as compared to the low-frequency residuals produced by STEP-1. This finding is similar to a study where spiral interleaves were reordered to minimize the influence of motion on dynamic imaging [27]. In this work, spiral interleaves were reordered, such that the alias-free region of the PSF is effectively enlarged for low and intermediate frequencies while sacrificing the high frequency alias-free regions.

Strong biases occur mainly in T1 maps. As the MRF sequence applies an inversion pulse in the beginning, the sensitivity to T1-related signal changes is very high in this early phase of the experiment. In an intuitive picture, a shift of residuals with low frequency and with a distinct minimum may cause a shift in time of the first zero crossing of the transverse magnetization and therefore significantly affect the T1 match. Whether the effect appears depends on the signal time course itself but also on the spatial location, which explains the observed artifact patterns within the object.

Our findings from the homogenous phantom were transferrable to in-vivo brain measurements. A pronounced spatial bias with the STEP 1 reordering can be mitigated with other STEP ILR schemes, where STEP-

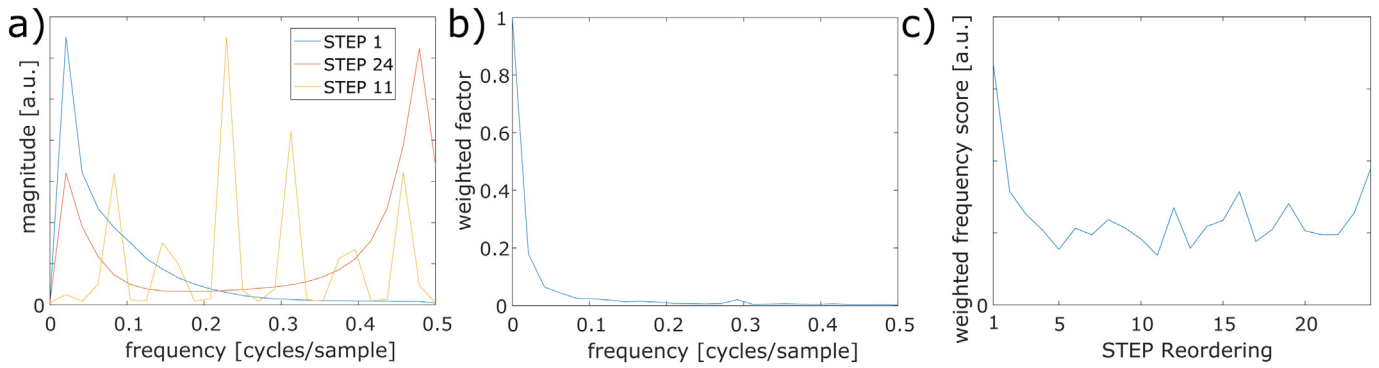

Fig. 3. a) Mean frequency spectrum of residuals from all pixels in the phantom from ascending (STEP-1), alternating (STEP-24) and STEP-11 reorderings. b) Function used for weighting the frequency spectrum of the residuals. c) Mean of weighted frequency score over residuals from all pixels in the phantom. Residuals were computed by reordering the sum of residuals according to STEP patterns. Weighted frequency score for STEP-1 to STEP-24 reorderings is shown. Higher values indicate that residuals have a relatively high amount of low-frequency components. STEP-11 turns out to be the best STEP reordering, based on this measure.

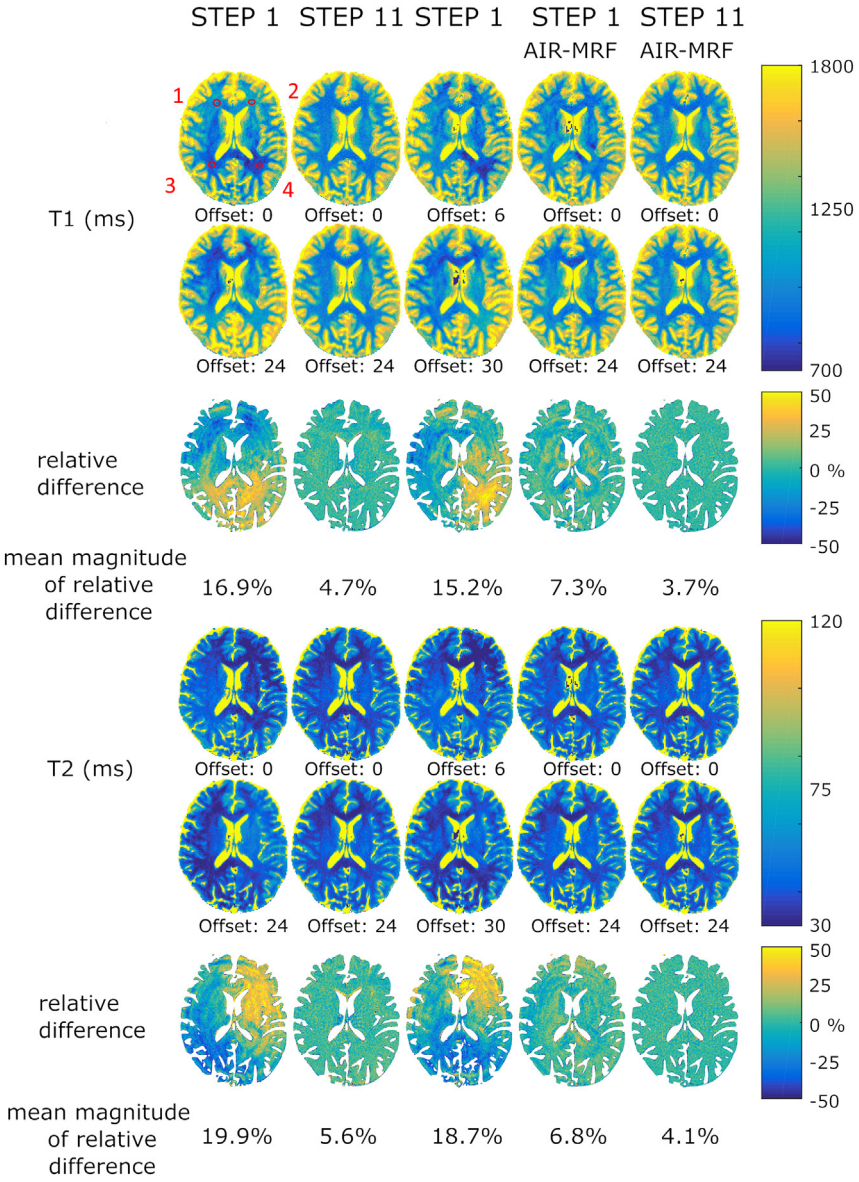

Fig. 4. MRF parameter maps and difference maps from dual density spiral MRF acquisitions using different ILR reorderings. T1 maps and the corresponding T2 maps are shown for different reorderings and offsets with and without AIR-MRF reconstruction,Respective shading maps, i.e. difference of the two parameter maps are shown for non fluid parts of the brain in the same column, together with the mean magnitude of the relative differences.

Table 1
Relaxation parameter values in the four ROIs in the brain.

	T1 in ROI 1 [ms]	T1 in ROI 2 [ms]	T1 in ROI 3 [ms]	T1 in ROI 4 [ms]
STEP–1 offset 0	1033 ± 66	1127 ± 45	825 ± 37	779 ± 26
STEP–1 offset 24	769 ± 27	816 ± 37	1082 ± 43	1062 ± 32
STEP–11 offset 0	897 ± 35	916 ± 45	934 ± 43	887 ± 33
STEP–11 offset 24	884 ± 31	906 ± 32	958 ± 28	903 ± 26
STEP–1 offset 6	961 ± 41	917 ± 38	971 ± 35	755 ± 42
STEP–1 offset 30	877 ± 32	825 ± 44	911 ± 29	1135 ± 28
STEP–1 offset 0	948 ± 42	921 ± 40	964 ± 40	922 ± 42
STEP–1 offset 24	877 ± 41	906 ± 25	949 ± 45	872 ± 21
STEP–11 offset 0	895 ± 37	903 ± 28	946 ± 31	919 ± 28
STEP–11 offset 24	903 ± 30	893 ± 29	950 ± 27	943 ± 33
	T2 in ROI 1 [ms]	**T2 in ROI 2 [ms]**	**T2 in ROI 3 [ms]**	**T2 in ROI 4 [ms]**
STEP–1 offset 0	35 ± 1.9	32 ± 2.2	43 ± 2.6	33 ± 2.3
STEP–1 offset 24	30 ± 1.3	40 ± 2.6	32 ± 1.5	37 ± 1.5
STEP–11 offset 0	32 ± 1.7	33 ± 1.9	37 ± 1.9	37 ± 2.1
STEP–11 offset 24	32 ± 1.4	33 ± 1.7	37 ± 1.6	37 ± 1.6
STEP–1 offset 6	33 ± 2.9	28 ± 2.2	44 ± 1.6	39 ± 3.3
STEP–1 offset 30	34 ± 1.2	39 ± 1.5	33 ± 2.2	34 ± 1.5
STEP–1 offset 0	34 ± 2.0	34 ± 1.5	37 ± 1.5	39 ± 1.5
STEP–1 offset 24	33 ± 1.9	36 ± 1.8	38 ± 1.9	36 ± 1.5
STEP–11 offset 0	33 ± 2.1	33 ± 1.3	37 ± 2.0	37 ± 1.4
STEP–11 offset 24	34 ± 1.8	33 ± 1.4	37 ± 1.7	38 ± 2.0

11 is giving the best results. This finding is confirmed by calculating difference maps: the map for the STEP-11 pattern has zero mean with low variation. Nevertheless, the effects of undersampling artifacts strongly depend on the underlying structure and in more complex body parts a different ILR pattern might be favorable.

Ideally, an optimized reordering scheme enables the generation of unbiased parameter maps with a simple and fast template matching algorithm, even if the signal is severely affected by k-space undersampling. More sophisticated reconstruction methods such as iterative reconstruction [11,12] or low rank [9,10] methods can minimize the spatial biases caused by undersampling artifacts. These types of methods can also benefit from optimized reordering schemes which could result in faster convergence and a substantial improvement of iterative methods that rely on pattern matches. However, it should be noted that reconstructions formulated as inverse problems do not necessarily have to be biased similarly as the simple pattern matching, as we have exemplarily shown for AIR-MRF. Differences in convergence are expected and potentially other ILR patterns might be better suited than the one found in this study.

This investigation does not cover the golden ratio reordering scheme that is used in a variety of MRF implementations [7,8], especially in those employing radial sampling [4,26]. However, a golden ratio reordering would correspond to a STEP ~14.83 scheme, which is very similar to STEP-15. Accordingly, it is not expected to provide significantly different results than the repetitive integer STEP reordering schemes investigated in this work. Nevertheless, golden angle reordering schemes also provide substantially better results than the originally proposed ascending reordering.

MRF can be implemented in various ways [4,6,8,26,28,29] [18] and a general solution to the optimization of MRF sequences [30] always has to be combined with the optimization of the sampling scheme. Insights gained in this work are nevertheless applicable to implementations of the fingerprinting concept with fingerprints that have similar frequency spectra and are expected to remain valid when using dictionary compression methods such as SVD compression [31]. The combination of low frequency signals and high frequency artifacts that we found to be favorable in our study is only a special case of the general problem to design signals and artifacts with different spectra. Future work is necessary to examine fingerprints with different spectra.

5. Conclusions

When applying undersampling of k-space in MRF, it is an essential and non-trivial task to ensure stable, bias-free results, which are not affected by the sampling pattern. It was shown, both by simulation and experiment, how an inadequate spiral interleaf reordering pattern will introduce a spatial bias to the MRF parameter maps. Investigating basic properties of the temporal interleaving scheme leads to objective criteria to identify the most appropriate sampling pattern, which was demonstrated in phantom and human-brain experiments.

Acknowledgements

The authors would like to thank Drs. Yun Jiang and Dan Ma (Department of Biomedical Engineering, Case Western Reserve University, Cleveland, Ohio, USA) for helpful discussions and Argyrios Kechagias (Siemens Healthcare, Erlangen) for supporting the phantom experiments.

Declaration of interest

G.K.: PhD program funding (Siemens Healthcare GmbH)
J.P., T.K., M.G., M.N.: employment (Siemens Healthcare GmbH)
B.H.: none
C.H.M.: Research support: Siemens Medical Solutions

References

[1] Margaret Cheng HL, Stikov N, Ghugre NR, Wright GA. Practical medical applications of quantitative MR relaxometry. J Magn Reson Imaging 2012;36:805–24. https://doi.org/10.1002/jmri.23718.
[2] Ma D, Gulani V, Seiberlich N, Liu K, Sunshine JL, Duerk JL, et al. Magnetic resonance fingerprinting. Nature 2013;495:187–92. https://doi.org/10.1038/nature11971.
[3] Jiang Y, Ma D, Seiberlich N, Gulani V, Griswold MA. MR fingerprinting using fast imaging with steady state precession (FISP) with spiral readout. Magn Reson Med 2015;74:1621–31. https://doi.org/10.1002/mrm.25559.
[4] Cloos MA, Knoll F, Zhao T, Block KT, Bruno M, Wiggins GC, et al. Multiparametric imaging with heterogeneous radiofrequency fields. Nat Commun 2016;7:12445. https://doi.org/10.1038/ncomms12445.
[5] Liao C, Bilgic B, Manhard MK, Zhao B, Cao X, Zhong J, et al. 3D MR fingerprinting with accelerated stack-of-spirals and hybrid sliding-window and GRAPPA reconstruction. NeuroImage 2017;162:13–22. https://doi.org/10.1016/j.neuroimage.2017.08.030.

[6] Chen Y, Jiang Y, Pahwa S, Ma D, Lu L, Twieg MD, et al. MR fingerprinting for rapid quantitative abdominal imaging. Radiology 2016;279:278–86. https://doi.org/10.1148/radiol.2016152037.
[7] Buonincontri G, Schulte RF, Cosottini M, Tosetti M. Spiral MR fingerprinting at 7 T with simultaneous B1 estimation. Magn Reson Imaging 2017;41:1–6. https://doi.org/10.1016/j.mri.2017.04.003.
[8] Hamilton JI, Jiang Y, Chen Y, Ma D, Lo W-C, Griswold M, et al. MR fingerprinting for rapid quantification of myocardial T_1, T_2, and proton spin density. Magn Reson Med 2017;77:1446–58. https://doi.org/10.1002/mrm.26216.
[9] Assländer J, Cloos MA, Knoll F, Sodickson DK, Hennig J, Lattanzi R. Low rank alternating direction method of multipliers reconstruction for MR fingerprinting. Magn Reson Med 2018;79:83–96. https://doi.org/10.1002/mrm.26639.
[10] Zhao B, Setsompop K, Ye H, Cauley SF, Wald LL. Maximum likelihood reconstruction for magnetic resonance fingerprinting. IEEE Trans Med Imaging 2016;35:1812–23. https://doi.org/10.1109/TMI.2016.2531640.
[11] Cline C, Chen X, Mailhe B, Wang Q, Nadar M. AIR-MRF: accelerated iterative reconstruction for magnetic resonance fingerprinting. Proc. 24th annu. meet. ISMRM, Singapore. 2016. p. 434.
[12] Pierre EY, Ma D, Chen Y, Badve C, Griswold MA. Multiscale reconstruction for MR fingerprinting. Magn Reson Med 2016;75:2481–92. https://doi.org/10.1002/mrm.25776.
[13] Pfeuffer J, Kechagias A, Körzdörfer G, Ma D, Griswold M, Nittka M. Mitigation of spiral undersampling artifacts in magnetic resonance fingerprinting (MRF) by adapted interleaf reordering. Proc. 25th annu. meet. ISMRM. 2017. p. 133.
[14] Körzdörfer G, Kluge T, Pfeuffer J, Griswold M, Jiang Y, Ma D, et al. Spatial biases in magnetic resonance fingerprinting parameter maps arising from undersampling patterns. Proc. 25th annu. meet. ISMRM. 2017. p. 3956.
[15] Pfeuffer J. Verbesserte Erzeugung von Bildpunkt-Zeit-Serien eines Untersuchungsobjektes mittels Magnetresonanztechnik. 2016:EP3299833.
[16] Meyer CH, Zhao L, Lustig M, et al. Dual-density and parallel spiral ASL for motion artifact reduction (PDF download available). Proc. 19th annu. meet. ISMRM 2011. p. 3986. https://doi.org/10.13140/RG.2.2.17527.62880.
[17] Tan H, Meyer CH. Estimation of *k*-space trajectories in spiral MRI. Magn Reson Med 2009;61:1396–404. https://doi.org/10.1002/mrm.21813.
[18] Buonincontri G, Sawiak SJ. MR fingerprinting with simultaneous B1 estimation. Magn Reson Med 2016;76:1127–35. https://doi.org/10.1002/mrm.26009.
[19] Gao Y, Chen Y, Ma D, Jiang Y, Herrmann KA, Vincent JA, et al. Preclinical MR fingerprinting (MRF) at 7 T: effective quantitative imaging for rodent disease models. NMR Biomed 2015;28:384–94. https://doi.org/10.1002/nbm.3262.
[20] Chung S, Kim D, Breton E, Axel L. Rapid B1 + mapping using a preconditioning RF pulse with turboFLASH readout. Magn Reson Med 2010;64:439–46. https://doi.org/10.1002/mrm.22423.
[21] Hong T, Kim M-O, Han D, Hwang D, Kim D-H. B1 inhomogeneity compensated MRF using simultaneous AFI. Proc. 23rd annu. meet. ISMRM. 2015. p. 3248.
[22] Ma D, Coppo S, Chen Y, McGivney D, Jiang Y, Pahwa S, et al. Slice profile and B1 corrections in 2D magnetic resonance fingerprinting. Magn Reson Med 2017. https://doi.org/10.1002/mrm.26580.
[23] Dydak U, Pruessmann KP, Weiger M, Boesiger P. The spatial response function in SENSE-SI. Proc. 8th annu. meet. ISMRM. 2000. p. 1848.
[24] Muja M, Lowe DG. Scalable nearest neighbor algorithms for high dimensional data n.d. doi:https://doi.org/10.1109/TPAMI.2014.2321376.
[25] Muja M, Lowe DG. Fast approximate nearest neighbors with automatic algorithm configuration. n.d.
[26] Assländer J, Glaser SJ, Hennig J. Pseudo steady-state free precession for MR-fingerprinting. Magn Reson Med 2017;77:1151–61. https://doi.org/10.1002/mrm.26202.
[27] Tsao J, Boesiger P, Pruessmann KP. Lattice permutation for reducing motion artifacts in radial and spiral dynamic imaging. Magn Reson Med 2006;55:116–25. https://doi.org/10.1002/mrm.20743.
[28] Ye H, Li Q, Cao X, Ding Q, He H, Liu H, et al. MR fingerprinting (MRF) incorporating simultaneous detection of RF transmit field and B0 inhomogeneity. Proc. 26th annu. meet. ISMRM. 2018. p. 172.
[29] Körzdörfer G, Jiang Y, Speier P, Pang J, Ma D, Pfeuffer J, et al. Magnetic resonance field fingerprinting. Magn Reson Med 2018. https://doi.org/10.1002/mrm.27558.
[30] Zhao Bo, Haldar JP, Setsompop K, Wald LL. Optimal experiment design for magnetic resonance fingerprinting. Conf Proc IEEE Eng Med Biol Soc 2016:453–6. https://doi.org/10.1109/EMBC.2016.7590737.
[31] McGivney DF, Pierre E, Ma D, Jiang Y, Saybasili H, Gulani V, et al. SVD compression for magnetic resonance fingerprinting in the time domain. IEEE Trans Med Imaging 2014;33:2311–22. https://doi.org/10.1109/TMI.2014.2337321.